scientific reports

Check for updates

OPEN

Remarkable enhancement of the adsorption and diffusion performance of alkali ions in two-dimensional (2D) transition metal oxide monolayers via Ru-doping

Shubham Sahoo[1], P. Kumari[1], Narayan N. Som[2], S. Kar[1], Rajeev Ahuja[3,4] & S. J. Ray[1]✉

Transition metal oxides (TMO) are the preferred materials for metal ion battery cathodes because of their high redox potentials and good metal-ion intercalation capacity, which serve as an outstanding replacement for layered sulphide. In this work, using first-principles calculations based on Density functional theory approach, we explored the structural and electronic properties which comprise of adsorption and diffusion behaviour along with the analysis of voltage profile and storage capacity of Ru doped two-dimensional transition metal oxide MnO_2, CoO_2, and NiO_2 monolayers. The adsorption of alkali ions (Li, Na) to the surface of TMOs is strengthened by Ru-atom doping. Ru doping enhanced the adsorption energy of Li/Na-ion by 25%/11% for MnO_2, 8%/13% for CoO_2, and 10%/11% NiO_2 respectively. The open circuit voltage (OCV) also increases due to the high adsorption capacity of doped Monolayers. Ru doping makes the semiconducting TMOs conduct, which is suitable for battery application. As alkali ion moves closer to the dopant site, the adsorption energy increases. When alkali ions are close to the vicinity of doping site, their diffusion barrier decrease and rises as they go further away. Our current findings will be useful in finding ways to improve the storage performance of 2D oxide materials for application in energy harvesting and green energy architecture.

The need for energy resources has grown significantly along with the quick growth of contemporary society. However, burning fossil fuels severely pollutes the environment and depletes non-renewable resources. As a result, it is becoming more and more necessary to find reusable and clean energy sources. Lithium-ion batteries (LIBs) are key components of many energy storage systems and offer a wide range of opportunities for the growth of new energy sectors[1]. The market for lithium-ion batteries (LIBs) as an electric energy source is expanding as a result of the meteoric rise in sales of electric vehicles and portable gadgets. However, the energy density and fast charging-discharging rate have limited their advancements[2]. The energy density of LIBs can be increased by using electrodes made of materials with high kinetics[3]. Therefore, research into novel materials with high-voltage profiles and high energy densities is urgently needed for energy harvesting[4].

A lot of two-dimensional (2D) materials have similar inherent benefits, for example, the abundant adsorption sites, short metal atom diffusion path, and great mechanical qualities with spin-transport functionality[5,6] etc. Moreover, large specific surfaces can facilitate ion adsorption and boost capacitance; high conductivity can quicken electron transport; configurable interlayer spacing is advantageous for ion intercalation and customizable active sites can exhibit electrocatalytic activity[7,8]. Due to all of these benefits, 2D materials are potential options for energy storage. 2D transition metal dichalcogenides (TMDs)[9,10], Janus materials[11] and transition metal oxides (TMOs)[12] with characteristic sandwiched structure of few atomic layers[13] have received a lot of

[1]Department of Physics, Indian Institute of Technology Patna, Bihta 801103, India. [2]Laboratory Nanostructures Institute of High Pressure Physics, Polish Academy of Sciences Sokolowska, Warsaw, Poland. [3]Department of Physics, Indian Institute of Technology Ropar, Rupnagar, Punjab 140001, India. [4]Condensed Matter Theory Group, Department of Physics and Astronomy, Uppsala University, SE-75120 Uppsala, Sweden. ✉email: ray@iitp.ac.in; ray.sjr@gmail.com

attention recently. Similar to graphene, some TMD materials, such as MoS_2[14], VS_2[15], WS_2[16], TiS_2[17], and SnS_2[18] that have a single layer or a few layers, have been suggested for usage as electrode materials in LIBs in both tests and theories. The cathode, one of the most crucial parts of metal-ion batteries, affects both the price and capacity of these batteries. Layered bulk metal oxides are currently utilized extensively in commercial LIBs. The creation of well-ordered structures is challenging, and the capacity is decreased by the bulk shapes of these layered materials.

2D oxide monolayers can offer remedies for these problems. Depending on the point-group symmetries, the oxide monolayers may have two different structures, such as 2H and 1T structures for D_6h and D_3d point-group symmetries, respectively[19]. Theoretically, MnO_2, CoO_2 and NiO_2 with the 1T structure are stable, according to Ataca et al.[20]. Among all the 2D materials, 2D TMOs show a large number of stabilised structures, just because the cations take on many charge states and binding configurations. 2D transition-metal oxide monolayers (MO_2; M = Mn, Co, and Ni)[12,21] have already been reported in the energy storage field as a cathode material for Li and Na ion batteries but they are not explored much in the context of rechargeable batteries. After the experimental synthesis of 2D MnO_2[22], it opens up many possibilities as an electrode for rechargeable batteries. Similarly, another 2D oxide RuO_2, although experimentally synthesised but underestimated in the context of electrode application. The reported 1T phase of RuO_2 monolayer[23] is half-metallic in nature with a high value of specific capacity with a decent voltage profile. RuO_2, SnO_2, and SnS_2 are already reported in Li-ion batteries applications[18], among which RuO_2 monolayer comes with various advantages.

Hetero-atom doping can alter the electrical and chemical properties of the parent structure[24,25]. For example, DFT calculations show a reduction in the ion-diffusion barrier and a narrowing of the bandgap (from insulator to semiconductor), resulting in significantly improved ion/electron conductivities of Mo doped $TiNb_2O_7$ micro rods[26]. Similarly, a very high capacity of 199 $mAh^1\ gm^{-1}$ and 235 $mAh^1\ gm^{-1}$ was obtained for the N-doped graphene and B-doped graphene[27–29]. After analysing the potential application of Ruthenium oxide (RuO_2) in the energy storage field in this work for the first time, we have doped Ruthenium(Ru) atom, in transition-metal oxide monolayers (MO_2; M = Mn, Co, and Ni). In this process of doping, we have substituted transition metal with Ru atom and we are taking the moderate doping percentage that is ~6% which can be archived by different chemical processes. We studied the electronic and structural properties where the adsorption of metal atoms at different active sites was systematically studied, along with the diffusion behaviour, specific capacity, and open circuit voltage was calculated by adopting the first principles based density functional theory approach.

Computational methods

First-principles based calculations were performed using Quantum ATK[30] which uses numerical linear combinations of atomic orbitals (LCAO) basis sets as implemented within Density functional theory approach. We have adopted the spin-polarized generalized gradient approximation (SGGA) using the Perdew-Burke-Ernzerhof parametrization technique (PBE technique) to take the electron exchange-correlation interactions[31] into consideration. In order to investigate the potential consequences of on-site Coulomb interaction of localized electrons in the investigated transition metals, we used DFT+U calculations[32,33]. A density mess cut-off of 125 in the Hartree unit was employed for the plane wave basis sets. A Monkhorst-Pack k-grid with a $5 \times 5 \times 1$ k-point mesh was adopted for geometry optimization. A 22 Å vacuum zone was applied in the out-of-plane direction to prevent interaction between periodic images. For structural relaxations, the energy and maximum force convergence criteria were set at 10^{-5} per atom and 0.01 eV $Å^{-1}$, respectively. In the process of calculating the band structure and density of states, the medium basic set with PseudoDojo pseudopotential was used, and a Monkhorst-Pack grid of $7 \times 7 \times 1$ points was used to build the Brillouin zone. The thermal stability of the pristine as well as metal atom adsorbed systems was addressed by performing Ab initio molecular dynamics (AIMD) calculations. To identify the charge transfer between the Metal-ion and TMOs monolayers, Bader charge analysis and isosurface charge density difference plot were performed with a densed $25 \times 25 \times 25$ FFT grid, where we calculated the charge transfer by plotting the isosurface plot. The climbing-image nudged elastic band (CI-NEB) approaches were utilized to identify the shortest energy pathway between the specified initial and final configurations in order to study the metal atom diffusion behaviour on the monolayer.

Results and discussion

Lattice structure and electronic properties of pristine transition-metal oxide monolayers (MO_2, M = Mn, Co, and Ni)

The monolayer has a D3d point-group symmetry and is in a sequence of an O-M-O layer that is three atoms thick where the Mn layer is sandwiched between two O layers[34]. The MnO_2, CoO_2, and NiO_2 monolayers can be grown by the molecular beam epitaxy method and these structures are comparable to transition metal dichalcogenides (TMD) in the T phase[35], where each transition metal atom occupies the centre of an octahedron made of six O atoms (Fig. 1a–c,g). The monolayers MnO_2[36] and NiO_2 are ferromagnetic semiconductors and we have calculated the band gap of 1.22 eV and 1.30 eV respectively. On the other hand, CoO_2 monolayer is magnetic and half-metallic in nature[37]. We took a $4 \times 4 \times 1$ supercell of monolayers

to design our structure which contains 48 atoms to save computational time. The projected density of states (PDOS) of MnO_2, CoO_2, and NiO_2 are shown in Fig. 1(d–f). The bond length between Manganese and Oxygen was taken to be 1.90 Å . The bond length between Co and oxygen and Ni and oxygen is set to be 1.88 Å . and 1.89 Å Fig. 1(a–c). The lattice parameter of MnO_2 is 11.26 Å and CoO_2 and NiO_2 are 11.29 Å respectively.

We have calculated the adsorption behaviour of pristine TMO monolayers by putting the alkali metal atom (Li and Na) on the monolayer's surface. For the adsorption behaviour, we took three favourable adsorption sites as shown in Fig. 1g. Among the adsorption sites, the B site is the metastable site, i.e. after optimization metal atom present on the B site comes to the T site whereas the metal atom present on H and T sites are representing stable

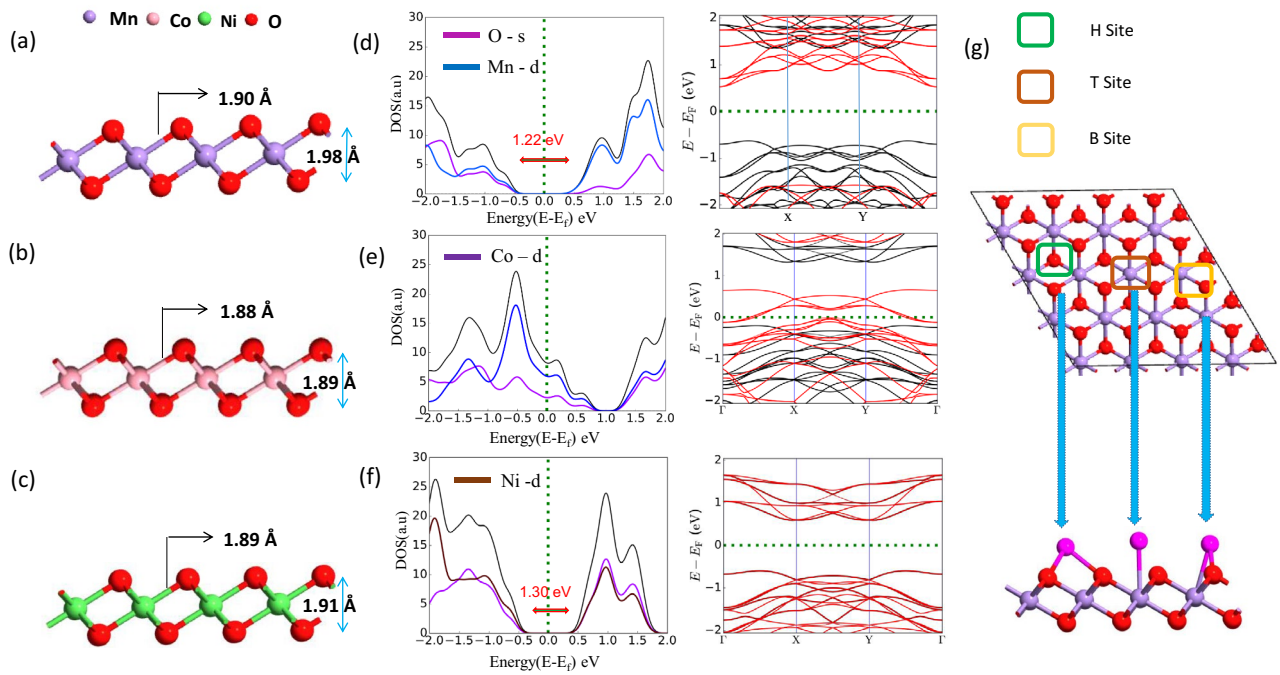

Figure 1. (**a**), (**b**) and (**c**) are the side view of pristine MnO_2, CoO_2, and NiO_2, (**d**), (**e**), (**f**) band structure and PDOS of MnO_2, CoO_2, and NiO_2 respectively, (**g**) possible adsorption sites for metal atom.

sites showing no displacement of the Li and Na atom after optimization. We have calculated the PDOS of single metal atom adsorbed on pristine TMO monolayers which are shown in Fig. S2[38] in the supporting information.

Structural, electronic properties and stability of the Ru doped 2D MnO_2, CoO_2, and NiO_2 monolayers

Before the analysis of electronic properties, the structural stabilities of all the monolayers should be explored after the substitution of transition metal atoms with Ru atoms. It was reported that it is possible to increase the catalytic activity of a host metal oxide by substituting a small portion of the cations with another cation also the transition metal (Fe, Co, Ni, and Cu)-doped α-MnO_2 nanowires[39] synthesized by a one-step hydrothermal method. So it opens up possibilities of doping in TMOs for different applications. We took into account a doping level of 6%, which is equivalent to doping one metal atom on a $4 \times 4 \times 1$ supercell (with 16 Transition metal atoms and 32 O atoms). For reference we have shown the horizontal view of the Ru doped CoO_2 monolayer in Fig. 2(e). One indicator of a structure's stability is formation energy which is calculated using the following equation[40].

$$E_{form} = E_{doped} - E_{pristine} + E_M - E_{Ru} \tag{1}$$

where E_{doped} is the total energy of the doped TMOs and $E_{pristine}$ is the total energy of undoped monolayers, E_M and E_{Ru} are the total energy of transition metal and Ru atom in its pure form respectively. The calculated formation energy for all the doped TMOs monolayers is negative indicating the stabilities of respective monolayers. The formation energy of all the monolayers is mentioned in Table 1. We also analysed the adsorption of the Ru atom on pristine monolayers and we conclude that the adsorption energy is more than the formation energy indicating doping is more suitable than the adsorption of the Ru atom. To explore the possibilities of stability of our structure, we have calculated the Phonon band structure shown in Fig. 2(a–c). As no negative frequency appears in the phonon dispersion in all the doped structures, they are found to be stable. However the thermal stability of the transition metal oxide (TMOs) monolayers is a major concern, so we have performed Ab initio molecular dynamics calculation at room tempreature to predict the thermal stabilities of the Ru doped TMOs monolayers Fig. (S6)[38]. From the AIMD calculations we can see the energy fluctuations are very small which indicate the stability at ambient tempreature. From the final structure of Ru doped MnO_2, We can see some extra bond present between Ru and Mn atom which were not present in the pristine monolayer. However for Ru doped CoO_2 and NiO_2 monolayer no such bonds were seen. Also, the bond length between Ru atom and the O atom appears to be more than the bond length of the previous Transition metal and O. Ru doping displays metallic properties, Ru atoms serve as electron donors and supply free electrons, resulting in higher electronic states in each case. We have also briefly studied the effect of Mo, Nb, and W doping in TMOs for analyzing the structural and electronic properties. The optimized Mo, Nb, and W-doped TMO structures are shown in Fig. S1[38]. of the supporting information.

Adsorption behavior of alkali metal atom

We first identify the most favorable position for a single metal atom adsorption on the monolayers in order to explore the nature of the adsorption of an alkali or alkaline earth metal M (= Li, Na) atom. From the symmetry

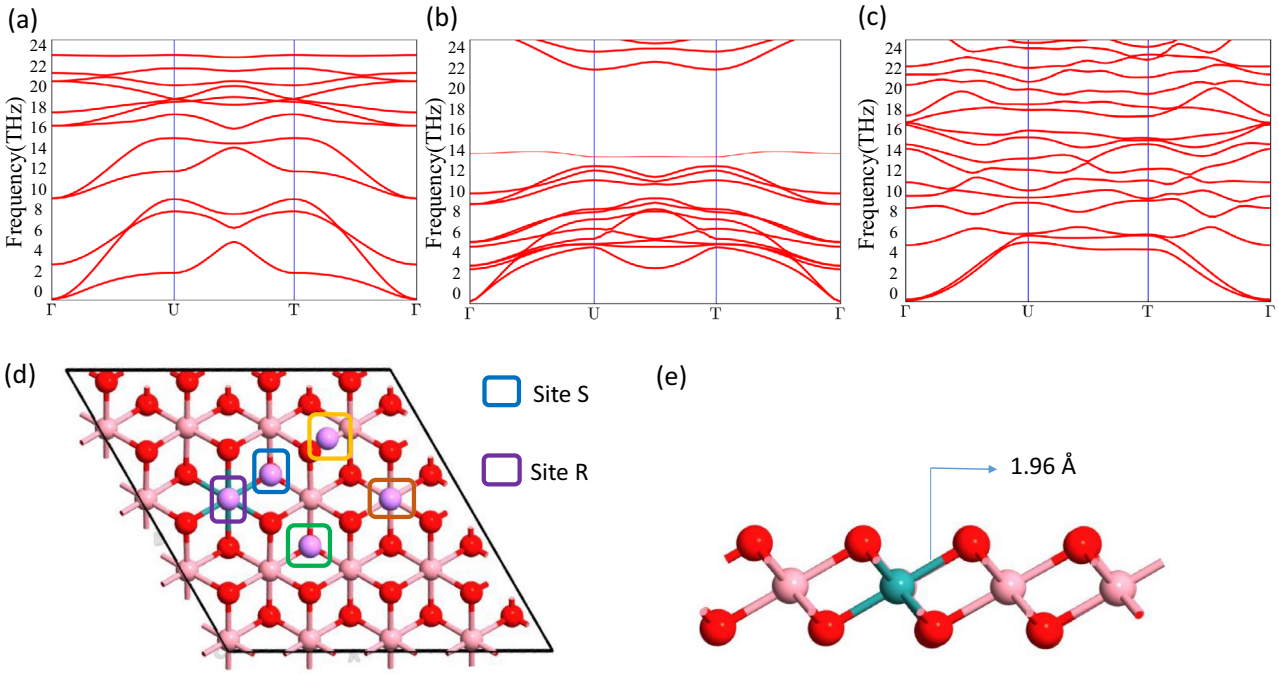

Figure 2. (**a**), (**b**), (**c**) Phonon Band structure of Ru doped 2D MnO_2, CoO_2, and NiO_2, (**d**) Horizontal view with possible adsorption sites, (**e**) Side view of doped monolayer.

TMO	d_{Li}(Å)	d_{Na}(Å)	E_{form} (eV)	E_{ad} (eV) Li/Na	ϵ (%) Li/Na	dQ(e) Li/Na
MnO_2	1.53	1.88	2.89	−3.07/-2.14	25/11	0.31/0.32
CoO_2	1.50	1.81	1.75	−3.64/-2.58	8/13	0.44/0 38
NiO_2	1.59	1.93	1.37	−3.16/-2.13	10/11	0.38/0.31

Table 1. adsorption distance of Li (d_{Li}) Åand Na (d_{Na}) atoms, on doped TMOs monolayer, Formation energies (E_{form}), adsorption energies E_{ad}(Li/Na), and the enhancement in adsorption ϵ (Li/Na) from pristine and dQ is the charge transfer in unit of e.

of the structure, we have considered two new adsorption sites (S site, R site) along with H, T, and B sites Fig. 2d. The metal atom present in H and R sites is bonded with three oxygen atoms i.e. hollow site (on an O atom in the bottom layer) whereas the metal atom present on S and T sites, one single bond can be seen between the metal atom and transition metal or doped atom. The adsorption energy was calculated with the following formula[41]

$$E_{ad} = \frac{E_{doped+M} - E_{doped} - nE_M}{n} \tag{2}$$

where $E_{doped+M}$ is the total energy of the doped TMOs with a single atom and $E_{pristine}$ is the total energy of undoped monolayers, E_M is the energy of the isolated metal atom, n is the number metal atoms. A more negative adsorption energy indicates a more favourable exothermic reaction between monolayer and metal atoms[42].

Site R is the energetically preferred adsorption site for all metal atoms due to the highest negative adsorption energy value whereas site H has the next higher energy followed by T site, indicating adsorption energy goes down when we leave the vicinity of the doped Ru atom. The R site can be attributed to the more number of M-O bonds (Three Metal atom-O bonds). Metal atoms will strongly adhere to the monolayer because of the extremely negative adsorption energies.

From Table 1 it was clear that Ru-doped TMO monolayers show enhancement in the adsorption of metal atoms. The adsorption energy of Ru doped MnO_2 increased from −2.29 eV of the pristine monolayer to −3.07 eV, similarly for doped CoO_2 and NiO_2 adsorption energy increased from −3.36 eV to −3.64 eV and −2.82 eV to −3.16 eV for Li and −1.89 eV to −2.14, −2.24 eV to 2.58 and −1.90 eV to −2.13 eV for Na atom respectively. These adsorption values are much greater than some well known electrode materials (FeSe[43], $NbSe_2$[44], phosphorene[45], borophene[46] and Janus monolayers[47,48]). Also, the increment of the percentage of adsorption energy is noted in Table 1 which was calculated using the following formula,

$$\epsilon = \frac{E(ad)_{doped} - E(ad)_{pristine}}{E(ad)_{doped}} \tag{3}$$

where $E(ad)_{doped}$ and $E(ad)_{pristine}$ are the adsorption energy on doped and pristine monolayers for metal atoms.

As concluded, for Ru-doped MnO_2 adsorption energy for Li atom is significantly increased (25%) indicating better intercalation. The adsorption distances of the alkali atoms from the monolayers are summarized in Table 1 where the adsorption distances d_{Li} and d_{Na}were measured from the top layer formed by O atoms. The Na atom adsorbed at a larger distance as compared to the Li atom for a particular monolayer. This can be confirmed from the charge transfer of Li and Na. As Na atom transfers less charge to the monolayer, we expect Na interacts weakly with the Ru doped monolayer as compared to Li. One of the expected reason is also that Na atom is larger in size as compared to Li atom, so Na needs larger space to accomodate in between the layers formed by Ru doped TMO monolayers. The adsorption energy of lithium and sodium on different adsorption sites is mentioned in Tables 2 and 3 respectively. We compared the adsorption energy of Li and Na for Nb, W, and Mo-doped TMOs which are mentioned in Fig. S4[38] in the SI. Comparing all the doping agents it was concluded that Ru doped TMOs show more enhancement of adsorption energy compared to others.

The isosurface plot of Li and Na adsorption on the Ru-doped monolayer surfaces is shown in Fig. 3 to visualize the adsorption process in more details. The charge transfer of Li/Na atom to Ru doped MnO_2, CoO_2 and NiO_2 on the R site are 0.31e/0.32e, 0.44e/0.38e and 0.38e/0.31e respectively which are confirmed from Brader charge analysis. According to the charge transfer of around 0.3e to 0.45e, there was a considerable electron transfer from the metal atom to the nearby O atoms, indicating a stronger bond between the metal atom and the TMO surface. The PDOS of single metal atom adsorbed in Ru-doped TMOs are shown the Fig. S3[38] in the SI. As the specific capacity and open circuit voltage are the outcome of full adsorption, we fill the structure with metal atoms on the R site first, which is the most favourable site, then on H Site, and optimized the structure for further calculation. To visualize the contribution of different orbitals to the density of states we have calculated the band structure and projected density of states for all the doped structures before and after the intercalation of metal atoms as shown in Fig. 4.

From PDOS it can be cleared that the d orbital of Mn, Co, Ni, and Ru whereas the s orbital of Li and Na are contributed significantly to the band structure. The PDOS of Mo, Nb, and W-doped TMO structures are given in Fig. S5[38] in the SI.

Diffusion of single metal atoms (Li and Na)

An essential metric for assessing electrode materials is the charge-discharge rate, which is mostly determined by the diffusion barrier of metal atoms[49]. Using the CI-NEB approach, we investigated the metal ion transport on the Ru-doped transition metal oxide monolayers. We took into consideration three different diffusion channels by analysing the symmetry and adsorption energy of TMO monolayers. Path 1 refers to the diffusion of metal ion from the R site to another R site via the B site of Ru and transition metal atom whereas path 2 and path 3 show the diffusion from H site to the R site and the H site to another H site via the B site respectively. B site as a metastable site serves as a channel for the diffusion process. We have calculated relative diffusion mobility using the Arrhenius equation. The diffusion constant (D) of Lithium and sodium ion can be calculated using the following equation[50].

$$D = D_0 e^{\frac{-E_b}{K_B T}} \tag{4}$$

where T is the ambient temperature, E_b is the barrier energy, k_B is Boltzmann's constant, and D_o is the temperature-independent pre-exponential constant and we took the D_o value same for all paths.

The calculated diffusion barrier for Path 1 is found to be the lowest among all other paths, representing metal atoms prefer to travel around the neighbourhood of Ru atom, the next preferable path is Path 2 followed by Path 3. The lowest diffusion barrier for the pristine MnO_2, CoO_2, and NiO_2 are found to be 0.5 eV, 0.6 eV, and 0.4 eV

Ru doped TMO	E_{ad} (R)	E_{ad} (H)	E_{ad} (S)	E_{ad} (T)
MnO_2	−3.07	−2.97	−2.89	−2.75
CoO_2	−3.64	−3.53	−3.37	−3.28
NiO_2	−3.16	−3.07	−2.90	−2.11

Table 2. Adsorption energy (eV) of lithium on different adsorption sites respectively.

Ru doped TMO	E_{ad} (R)	E_{ad} (H)	E_{ad} (S)	E_{ad} (T)
MnO_2	−2.14	−2.10	−2.07	−2.00
CoO_2	−2.58	−2.44	−2.33	−2.20
NiO_2	−2.13	−2.07	−1.97	−1.85

Table 3. Adsorption energy (eV) of sodium on different adsorption sites respectively.

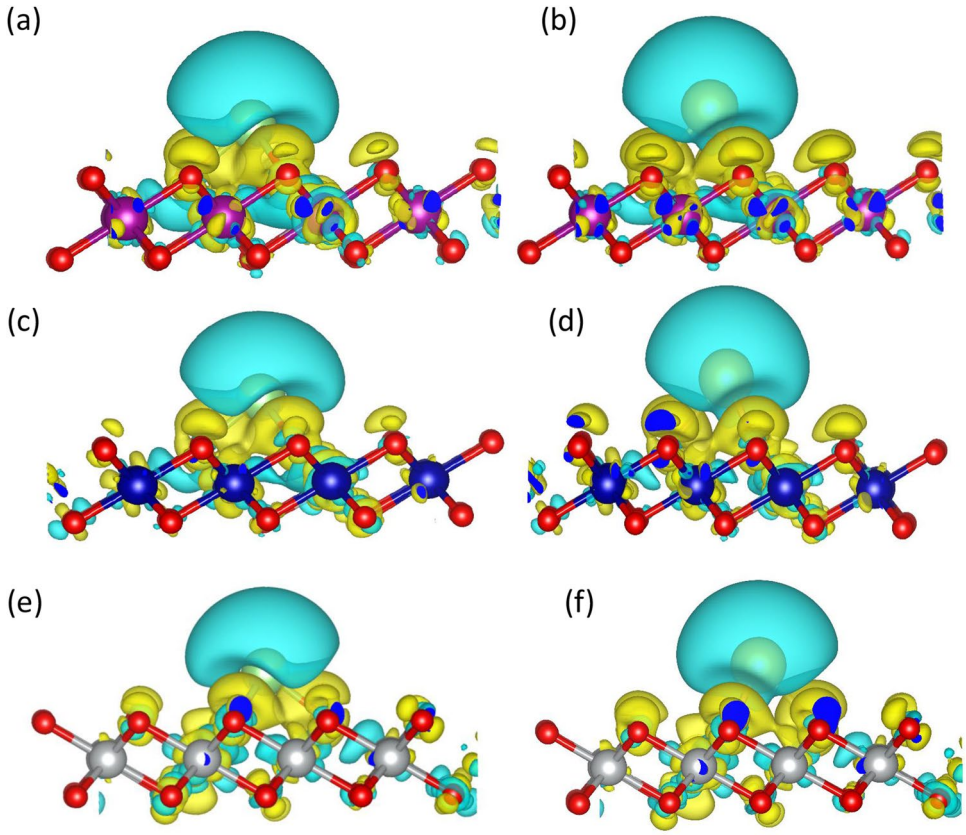

Figure 3. (**a**), (**b**) iso-surface plot for Li and Na adsorbed Ru doped MnO_2 (**c**), (**d**) and (**e**), (**f**) iso-surface plot for Li and Na adsorbed Ru doped CoO_2 and NiO_2 monolayers respectively. Yellow and cyan colors represent electron accumulation and electron depletion regions respectively.

respectively whereas, for the Ru-doped TMOs, the diffusion barrier is found to be 0.35 eV, 0.42 eV, 0.52 eV for Li-ion and 0.11 eV, 0.28 eV and 0.42 eV for Na atom respectively which indicates that doping lowers the barrier to promote fascinating ion diffusion.

The calculated diffusion barrier for all the paths for Li and Na are mentioned in Table 4. The diffusion barrier for sodium is found to be less than the diffusion barrier for lithium. This was expected for the larger adsorption distance of Na as compared to lithium. The diffusion barrier of alkali metal atoms on different paths is shown in Fig. 5. The calculated diffusion barrier for our system is lower than the some of the well reported structure Mg_3N_2[51], B_3S[52].These small barrier allow the fast movement of the metal atom which in turn fasten the charging capability.

Open circuit voltage and specific capacity

It is necessary for the cathode materials to work in conjunction with electrodes in applications because they are one of the key elements of lithium-ion batteries. The positive electrode (Cathode) must have a comparatively high open-circuit voltage in order to create a high electric potential[53,54]. To ensure higher output voltage, the positive electrode material frequently needs to: (i) have high and stable potential, (ii) maintain its structural stability after full adsorption of metal atoms during charging, (iii) have higher specific capacity. By analysing the properties while gradually increasing metal atoms, these two properties are evaluated. We used the $4 \times 4 \times 1$ supercell of the monolayers as the substrate.

which allowed us to make changes in the charging process to the adsorption of metals on both sides of the monolayers until it achieves its full capacity. The interaction between the adsorbed layers caused the absolute value of the average adsorption energy to steadily decrease as the amount of Li increased. The change of open circuit voltage with the metal atom content is shown in Fig. 6. The OCVs of Li and Na atoms are calculated according to the following equation by using average adsorption energy, E_{ad} of n metal atoms adsorbed system, and e is the charge of an electron.

$$OCV = -\frac{E_{ad}}{e} \tag{5}$$

where E_{ad} is the average adsorption energy of a metal atom and e is the charge of an electron.

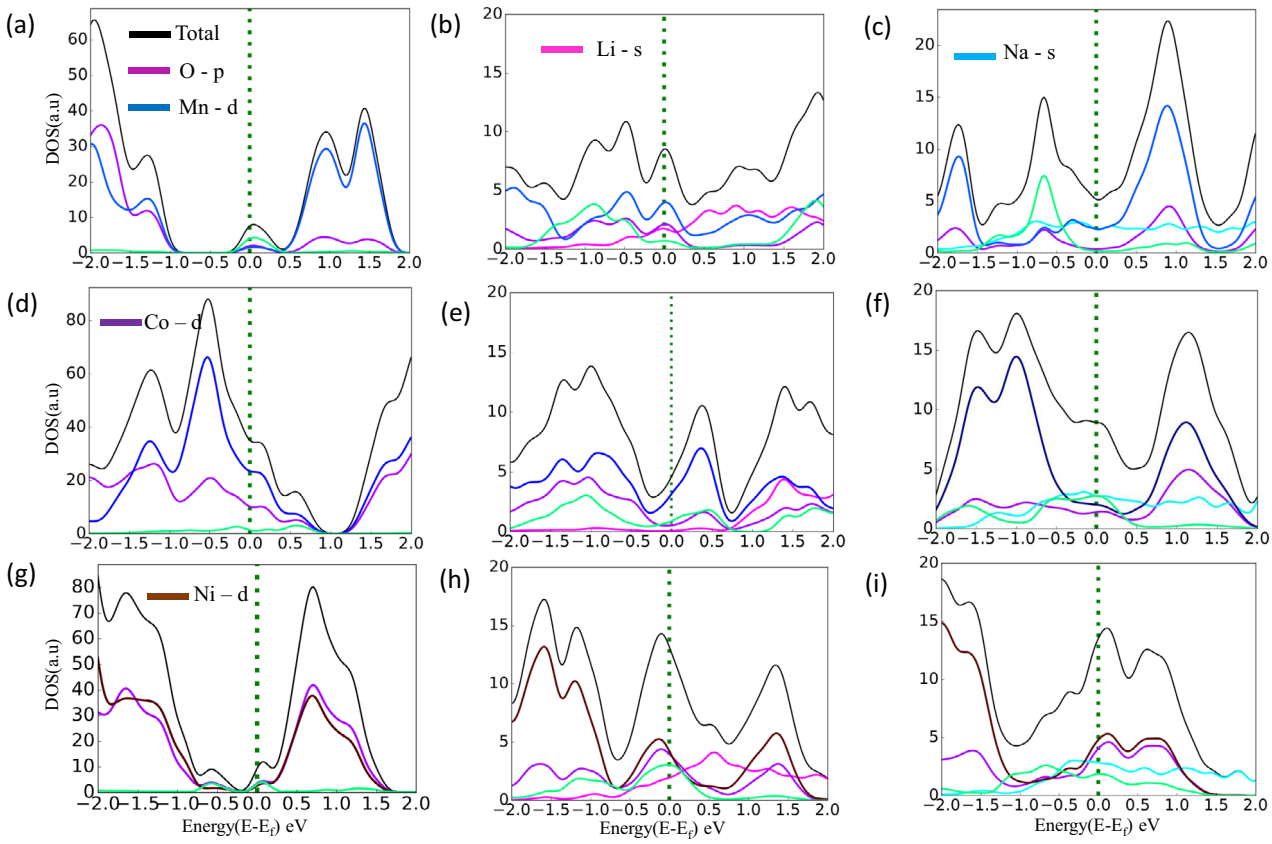

Figure 4. (**a**), (**b**), (**c**) PDOS of Ru doped MnO_2 without intercalation and Full Lithium and Sodium intercalated structure (**d**), (**e**), (**f**) and (**g**), (**h**) and (**i**) represent PDOS of Ru doped CoO_2 and NiO_2 monolayer without and full intercalation of Li and Na atom respectively.

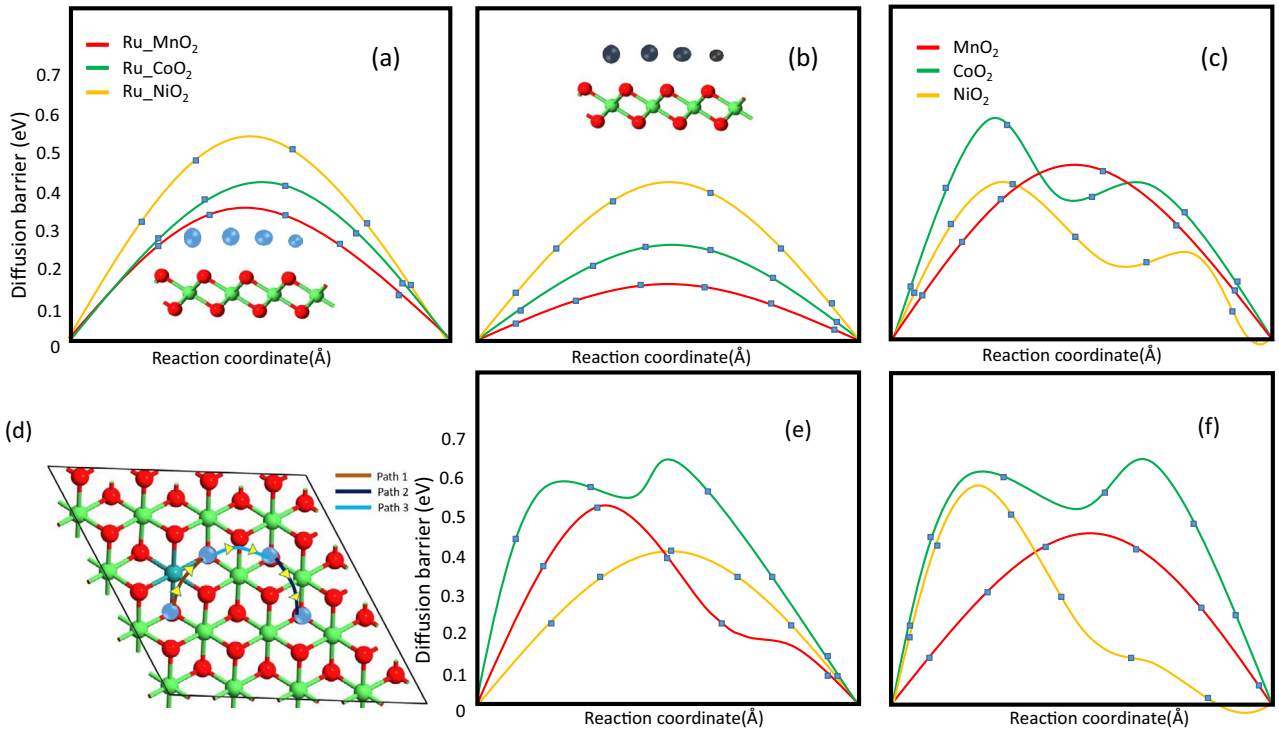

Figure 5. (**a**), (**b**) represent Diffusion barrier on Ru doped TMOs monolayers along path 1 for Li and Na respectively, (**c**) lowest diffusion barrier of pristine TMOs, (**d**) visualization of diffusion path (**e**), (**f**) diffusion barrier of Li and Na through path 2.

Ru doped TMO	E_b (Path 1) (Li/Na)	E_b (Path 2) (Li/Na)	E_b (Path 3) (Li/Na)
Ru-MnO_2	0.35/0.10	0.50/0.30	0.40/0.22
Ru-CoO_2	0.40/0.20	0.70/0.30	0.70/0.30
Ru-NiO_2	0.50/0.40	0.40/0.30	0.58/0.30

Table 4. Calculated diffusion barrier(E_b) eV for 3 different paths for Li and Na.

Pristine TMO	O.C.V (Li/Na)	Ru doped TMO	O.C.V (Li/Na)
MnO_2	1.87/1.1	MnO_2	2.02/1.23
CoO_2	2.10/1.31	CoO_2	2.30/1.35
NiO_2	2.30/1.34	NiO_2	2.43/1.43

Table 5. Comparision of O.C.V (Volt) between pristine and doped structure.

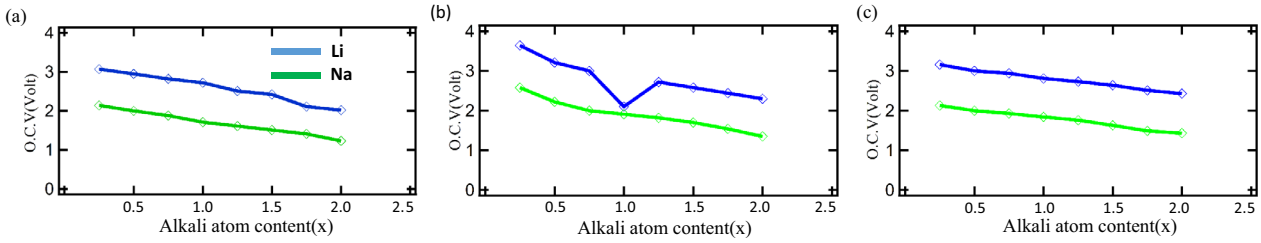

Figure 6. (**a**), (**b**), (**c**) Open circuit voltage Vs content of Li and Na atom in Ru doped MnO_2, CoO_2 and NiO_2 respectively.

The calculated O.C.V for all three Ru-doped monolayers is mentioned in Table 5. It was clear that Ru-doped MnO_2, CoO_2, and NiO_2 showed enhancement in cell voltage as compared to pristine monolayers, which is a desirable feature for the next-generation cathode material. However some article have followed different apporach to calculate the O.C.V which we have discussed in the last section of the supplimentary information in Fig. S9[38]. The specific capacity for Lithium and Sodium storage can be estimated using the following equation,

$$C = \frac{xnF}{M + nM_m} \tag{6}$$

Here M is the molecular weight of doped monolayers, M_m is the molecular mass of the metal atom and F is the Faraday constant of 26801 mAhmol^{-1}, x is the chemical stoichiometry of the metal atom and n is the valency of lithium and sodium ion i.e n=1 for Lithium and Sodium, n=2 for potassium, Calcium.

The increased Li concentration provides more repulsive interaction, therefore the Li adsorption energy steadily declines as x increases. The metal atom concentration in the Ru-doped TMO monolayers reaches the maximum value, which corresponds to the case of x = 2 in Li/Na_xMO_2. At this stage the calculated specific capacity for Ru doped MnO_2, CoO_2, and NiO_2 are 453 mAhgm^{-1}/361 mAhgm^{-1}, 442 mAhgm^{-1}/357 mAhgm^{-1} and 441 mAhgm^{-1}/355 mAhgm^{-1}for Li/Na. Thermal stability of the electrode material after full lithiation and sodiation is most important. To check the thermal stability at room temperature we have performed Ab initio molecular dynamics (AIMD) calculations. The AIMD calculation results for full lithium and sodium intercalated system for all three Ru-doped 2D MnO_2, CoO_2, and NiO_2 monolayers are shown in Figs. S7, S8[38]. We observed a very little energy fluctuation, so the structures are expected to be stable.

Conclusion

We have thoroughly analyzed the performance of pristine and Ru-doped 2D MnO_2, CoO_2, and NiO_2 monolayers as cathode material for lithium- and sodium-ion batteries using DFT calculation. Our findings reveal that Ru doping enhanced the adsorption energy of the monolayers. MnO_2 showed the highest 25% increment in adsorption while CoO_2 and NiO_2 showed an enhancement of 13% and 11% respectively which represent strong binding of alkali ions as compared to pristine monolayers. The adsorption energy increases when one approaches towards the doping site and decreases when one moved away from the doping site showing doping sites are more favourable for metal atom binding. We have also calculated the diffusion barrier along different paths among which metal atoms prefer the path through the vicinity of the doped agent referring to doping facilitating the diffusion process. The lowest barrier for doped MnO_2, CoO_2, and NiO_2 are 0.35 eV/0.14 eV, 0.5 eV/0.3 eV and 0.4 eV/0.22 eV for Li/Na atom respectively. Our findings showed that Ru atom doping can significantly enhance

the adsorption and diffusion properties of Transition metal oxide monolayers, making them desirable materials for cathodes in alkali-ion rechargeable batteries.

Supporting information

The Supporting Information is available here, which contains additional information/data related to teh claims made in the main article[38].

Data availability

The data that support the findings of this study are available from the corresponding author(s) upon reasonable request.

Received: 19 October 2023; Accepted: 7 February 2024
Published online: 22 February 2024

References

1. Li, J., Daniel, C. & Wood, D. Materials processing for lithium-ion batteries. *J. Power Sources* **196**(5), 2452–2460 (2011).
2. Feng, S., Hou, X., Qin, J. & Zhong-Shuai, W. Recent advances and challenges of two-dimensional materials for high-energy and high-power lithium-ion capacitors. *Batter. Supercaps* **3**(1), 10–29 (2020).
3. Ye, C. *et al.* Unveiling the advances of 2D materials for Li/Na-S batteries experimentally and theoretically. *Matter* **2**(2), 323–344 (2020).
4. Gupta, N., Rani, S., Kumari, P., Ahuja, R. & Ray, S. J. Ultralow lattice thermal conductivity and thermoelectric performance of twisted graphene/boron nitride heterostructure through strain engineering. *Carbon* **215**, 118437 (2023).
5. Chen, K.-S., Balla, I., Luu, N. S. & Hersam, M. C. Emerging opportunities for two-dimensional materials in lithium-ion batteries. *ACS Energy Lett.* **2**(9), 2026–2034 (2017).
6. Rani, S., Nair, A. K., Venkata Kamalakar, M. & Jyoti Ray, S. Spin-selective response tunability in two-dimensional nanomagnet. *J. Phys.: Condens. Matter* **32**(41), 415301 (2020).
7. Liu, T., Ding, J., Zhiqiang, S. & Wei, G. Porous two-dimensional materials for energy applications: Innovations and challenges. *Materials Today Energy* **6**, 79–95 (2017).
8. Mukherjee, S. & Singh, G. Two-dimensional anode materials for non-lithium metal-ion batteries. *ACS Appl. Energy Mater.* **2**(2), 932–955 (2019).
9. Pi, L. *et al.* Recent progress on 2D noble-transition-metal dichalcogenides. *Adv. Func. Mater.* **29**(51), 1904932 (2019).
10. Ray, S. J. First-principles study of MoS_2, phosphorene and graphene based single electron transistor for gas sensing applications. *Sens. Actuators, B Chem.* **222**, 492–498 (2016).
11. Kar, S., Kumari, P., Venkata Kamalakar, M. & Ray, S. J. Twist-assisted optoelectronic phase control in two-dimensional (2D) Janus heterostructures. *Sci. Rep.* **13**(1), 13696 (2023).
12. Leong, C. C., Pan, H. & Ho, S. K. Two-dimensional transition-metal oxide monolayers as cathode materials for Li and Na ion batteries. *Phys. Chem. Chem. Phys.* **18**(10), 7527–7534 (2016).
13. Sachin, S. *et al.* Van der Waals twistronics in a MoS_2/WS_2 heterostructure. *Comput. Condens. Matter* **35**, e00797 (2023).
14. Liu, T. *et al.* A density functional theory study of high-performance pre-lithiated MS_2 (M= Mo, W, V) monolayers as the anode material of lithium ion batteries. *Sci. Rep.* **10**(1), 6897 (2020).
15. Wang, D. *et al.* Two-dimensional vs 2 monolayers as potential anode materials for lithium-ion batteries and beyond: First-principles calculations. *J. Mater. Chem. A* **5**(40), 21370–21377 (2017).
16. Yelgel, C. E. L. A. L., Yelgel, Ö. C. & Gülseren, O. Structural and electronic properties of MoS_2, WS_2, and WS_2/MoS_2 heterostructures encapsulated with hexagonal boron nitride monolayers. *J. Appl. Phys.* **122**(6), 065303 (2017).
17. Li, S. N., Liu, J. B. & Liu, B. X. First principles study of nanostructured TiS_2 electrodes for Na and Mg ion storage. *J. Power Sources* **320**, 322–331 (2016).
18. Hassan, A. S., Moyer, K., Ramachandran, B. R. & Wick, C. D. Comparison of storage mechanisms in RuO_2, SnO_2, and SnS_2 for lithium-ion battery anode materials. *J. Phys. Chem. C* **120**(4), 2036–2046 (2016).
19. Rasmussen, F. A. & Thygesen, K. S. Computational 2D materials database: Electronic structure of transition-metal dichalcogenides and oxides. *J. Phys. Chem. C* **119**(23), 13169–13183 (2015).
20. Ataca, C., Sahin, H. & Ciraci, S. Stable, single-layer MX_2 transition-metal oxides and dichalcogenides in a honeycomb-like structure. *J. Phys. Chem. C* **116**(16), 8983–8999 (2012).
21. Sahoo, S., Kumari, P. & Jyoti Ray, S. Promising cathode material MnO_2/CoO_2 heterostructure for the Li and Na ion battery: A computational study. *J. Appl. Phys.* **134**(10), 104302 (2023).
22. Omomo, Y., Wang, T. S. & Watanabe, M. Redoxable nanosheet crystallites of MnO_2 derived via delamination of a layered manganese oxide. *J. Am. Chem. Soc.* **125**(12), 3568–3575 (2003).
23. Ko, D.-S. *et al.* Understanding the structural, electrical, and optical properties of monolayer h-phase RuO_2 nanosheets: A combined experimental and computational study. *NPG Asia Mater.* **10**(4), 266–276 (2018).
24. Ray, S. J. & Venkata Kamalakar, M. Unconventional strain-dependent conductance oscillations in pristine phosphorene. *Phys. Chem. Chem. Phys.* **20**(19), 13508–13516 (2018).
25. Rani, S. & Ray, S. J. Two-dimensional C3N based sub-10 nanometer biosensor. *Phys. Chem. Chem. Phys.* **22**(20), 11452–11459 (2020).
26. Lei, C., Qin, X., Huang, S., Wei, T. & Zhang, Y. Mo-doped $Tinb_2O_7$ microspheres as improved anode materials for lithium-ion batteries. *ChemElectroChem* **8**(17), 3379–3383 (2021).
27. Yao, L.-H. *et al.* Adsorption of Na on intrinsic, B-doped, N-doped and vacancy graphenes: A first-principles study. *Comput. Mater. Sci.* **85**, 179–185 (2014).
28. Riyaz, M., Garg, S., Kaur, N. & Goel, N. Boron doped graphene as anode material for Mg ion battery: A DFT study. *Comput. Theor. Chem.* **1214**, 113757 (2022).
29. Zhong-Shuai, W., Ren, W., Li, X., Li, F. & Cheng, H.-M. Doped graphene sheets as anode materials with superhigh rate and large capacity for lithium ion batteries. *ACS Nano* **5**(7), 5463–5471 (2011).
30. Smidstrup, S. *et al.* Quantumatk: An integrated platform of electronic and atomic-scale modelling tools. *J. Phys.: Condens. Matter* **32**(1), 015901 (2019).
31. Sham, L. J. Exchange and correlation in density-functional theory. *Phys. Rev. B* **32**(6), 3876 (1985).
32. Kar, S., Rani, S. & Ray, S. J. Stimuli assisted electronic, magnetic and optical phase control in CrOBr monolayer. *Physica E* **143**, 115332 (2022).
33. Kumari, P., Rani, S., Kar, S., Venkata Kamalakar, M. & Ray, S. J. Strain-controlled spin transport in a two-dimensional (2D) nano-magnet. *Sci. Rep.* **13**(1), 16599 (2023).

34. Chu, V.-H., Le, T.-H., Pham, T.-T. & Nguyen, D.-L. Phonon transport in Janus monolayer siblings: A comparison of 1T and 2H-ISbTe. *RSC Adv.* **13**(7), 4202–4210 (2023).
35. Yang, X., Singh, D., Zhitong, X., Wang, Z. & Ahuja, R. An emerging Janus MoSeTe material for potential applications in optoelectronic devices. *J. Mater. Chem. C* **7**(39), 12312–12320 (2019).
36. Wines, D., Saritas, K. & Ataca, C. Intrinsic ferromagnetism of two-dimensional (2D) MnO_2 revisited: A many-body quantum monte Carlo and DFT+ u study. *J. Phys. Chem. C* **126**(13), 5813–5821 (2022).
37. Bandyopadhyay, A., Li, S. & Frauenheim, T. Role of external stimuli in engineering magnetic phases and real-time spin dynamics of Co/Mn oxides. *J. Phys. Chem. Lett.* **13**(29), 6755–6761 (2022).
38. Sahoo, S., Kumari, P., Som, N. N., Ahuja, R. & Ray, S. J. Supporting information of remarkable enhancement of the adsorption and diffusion performance of alkali ions in two dimensional (2D) transition metal oxide monolayers via Ru-doping (2024).
39. Umar, A. *et al.* Single crystalline α-manganese dioxide (α-MnO_2) nanowires as anode materials for lithium-ion batteries. *Mater. Express* **12**(12), 1560–1565 (2022).
40. Nair, A. K., Da Silva, C. M. & Amon, C. H. Tuning the adsorption and diffusion capabilities of titanium disulfide monolayers by doping and strain engineering: Implications for lithium-ion batteries. *Appl. Surf. Sci.* **600**, 154164 (2022).
41. Al Roman, A., Rahman, M. M., Hossain, K., Das, S. & Ahmed, F. Development of high-performance ScS_2 monolayer as cathode material: A DFT analysis. *Solid State Commun.* **352**, 114828 (2022).
42. Bekeur, C. A. & Mapasha, R. E. Enhancement of electrochemical performance of monolayer SnS_2 for Li/Na-ion batteries through a Sulphur vacancy: A DFT study. *J. Solid State Electrochem.* **27**, 2445–2456 (2023).
43. Lv, X. *et al.* Metallic FeSe monolayer as an anode material for Li and non-Li ion batteries: A DFT study. *Phys. Chem. Chem. Phys.* **22**(16), 8902–8912 (2020).
44. Lv, X., Wei, W., Sun, Q., Huang, B. & Dai, Y. A first-principles study of $NbSe_2$ monolayer as anode materials for rechargeable lithium-ion and sodium-ion batteries. *J. Phys. D Appl. Phys.* **50**(23), 235501 (2017).
45. Sibari, A. *et al.* Phosphorene as a promising anode material for (Li/Na/Mg)-ion batteries: A first-principle study. *Sol. Energy Mater. Sol. Cells* **180**, 253–257 (2018).
46. Jena, N. K., Araujo, R. B., Shukla, V. & Ahuja, R. Borophane as a benchmate of graphene: A potential 2D material for anode of Li and Na-ion batteries. *ACS Appl. Mater. Interfaces.* **9**(19), 16148–16158 (2017).
47. Xiong, F. & Chen, Y. A first-principles study of Janus monolayer TiSSe and VSSe as anode materials in alkali metal ion batteries. *Nanotechnology* **32**(2), 025702 (2020).
48. Shang, C. *et al.* Theoretical prediction of Janus MoSSe as a potential anode material for lithium-ion batteries. *J. Phys. Chem. C* **122**(42), 23899–23909 (2018).
49. Zhao, R. X., Wan, C. B., Qian, P. & Xin, J. Insight into the effects of S-vacancy and O-doping in monolayer VS_2 as lithium-ion battery anodes from first-principles calculations. *Surf. Interfaces* **38**, 102851 (2023).
50. Oukahou, S., Elomrani, A., Maymoun, M., Sbiaai, K. & Hasnaoui, A. Investigation of $LiMn_{1-x}M_xPO_4$ (M= Ni, Fe) as cathode materials for li-ion batteries using density functional theory. *Comput. Mater. Sci.* **202**, 111006 (2022).
51. Xiong, L. *et al.* Density functional theory prediction of Mg 3 N 2 as a high-performance anode material for Li-ion batteries. *Phys. Chem. Chem. Phys.* **21**(13), 7053–7060 (2019).
52. Jana, S., Thomas, S., Lee, C. H., Jun, B. & Lee, S. U. B 3 S monolayer: Prediction of a high-performance anode material for lithium-ion batteries. *J. Mater. Chem. A* **7**(20), 12706–12712 (2019).
53. Liang, B., Ma, N., Wang, Y., Wang, T. & Fan, J. N-functionalized Ti_2B MBene as high-performance anode materials for sodium-ion batteries: A DFT study. *Appl. Surf. Sci.* **599**, 153927 (2022).
54. Patel, P. *et al.* Two-dimensional α-SiX (X= N, P) monolayers as efficient anode material for Li-ion batteries: A first-principles study. *ACS Appl. Nano Mater.* **6**(3), 2103–2115 (2023).

Author contributions

S.S. wrote the manuscript. All authors reviewed the manuscript.

Competing interests

The authors declare no competing interests.

Additional information

Supplementary Information The online version contains supplementary material available at https://doi.org/10.1038/s41598-024-53966-5.

Correspondence and requests for materials should be addressed to S.J.R.

Reprints and permissions information is available at www.nature.com/reprints.

Publisher's note Springer Nature remains neutral with regard to jurisdictional claims in published maps and institutional affiliations.

Open Access This article is licensed under a Creative Commons Attribution 4.0 International License, which permits use, sharing, adaptation, distribution and reproduction in any medium or format, as long as you give appropriate credit to the original author(s) and the source, provide a link to the Creative Commons licence, and indicate if changes were made. The images or other third party material in this article are included in the article's Creative Commons licence, unless indicated otherwise in a credit line to the material. If material is not included in the article's Creative Commons licence and your intended use is not permitted by statutory regulation or exceeds the permitted use, you will need to obtain permission directly from the copyright holder. To view a copy of this licence, visit http://creativecommons.org/licenses/by/4.0/.

© The Author(s) 2024